Trans. JSASS Aerospace Tech. Japan
Vol. 14, No. ists30, pp. Pe_95-Pe_104, 2016

Study of the Effects of Heat Load, Ablator Density and Backup Structure upon the Thermal Protection Performance of Heat Shield Systems Consisting of Phenolic Carbon Ablators

By Sumio KATO,[1)] Shoichi MATSUDA,[1)] Keiichi OKUYAMA,[2)] Kenta GIBO,[3)] Hiroaki OYA,[4)] Akihiro WATANABE,[1)] Naoyuki SHIMADA[1)] and Shunsuke SAKAI[1)]

[1)]*University of the Ryukyus, Nishihara, Japan*
[2)]*Kyushu Institute of Technology, Kitakyushu, Japan*
[3)]*Okinawa National College of Technology, Nago, Japan*
[4)]*Kawasaki Heavy Industries, Ltd., Kobe, Japan*

(Received August 3rd, 2015)

The effects of heat load, ablator density, and backup structure, etc. upon the heat shield performance of the lightweight phenolic carbon ablators named LATS were investigated using a one-dimensional ablation analysis code. The ablator density was assumed to be from about 260 to 1000kg/m^3. Heat flux time histories of a rectangular pattern were assumed, where cases of constant heating duration time and constant accumulated heat load (up to 600MJ/m^2) were considered. The heating level was assumed to be from 1 to 10MW/m^2, which means that the ablator surface is in the region of diffusion control oxidation/sublimation. The materials of the backup wall are assumed to be aluminum, stainless steel and high density CFRP. Main findings are: (1) For a low heat flux q with the same heating duration time t_q, the necessary thickness, with which the maximum back surface temperature equals to the pre-determined allowable temperature, is nearly constant as the density ρ_v changes. On the other hand, the necessary thickness increases largely when q is larger and ρ_v is smaller. The ablator necessary mass increases with the increase of ρ_v and q for the same t_q. (2) When a backup wall is attached, the necessary thickness decreases and the necessary mass including the wall mass increases. (3) For a constant accumulated heat load, necessary thickness and mass decrease for a higher heat flux q especially when ρ_v is high. (4) A lower density ablator with a CFRP backup wall gives the lightest mass of the heat shield system for most of the parameter range among the three wall materials. (5) For a high heat flux, selection of a lower density ablator gives a larger necessary thickness.

Key Words: **A**blator, Heat Shield System, Re-Entry Capsule, Ablation Analysis

Nomenclature

C_p	:	specific heat, J/(kg K)
h	:	enthalpy, J/kg
k	:	thermal conductivity, W/(m K)
L_1	:	length of ablator, m
L_2	:	thickness of backup wall, m
m_{ne}	:	necessary mass of ablator, kg/m^2
m_{neALL}	:	$m_{ne}+m_2$, kg/m^2
m_2	:	mass density of backup wall, kg/m^2
$\dot{m}$	:	mass flux, kg/(m^2 s)
Q	:	accumulated heat load, MJ/m^2
q	:	heat flux, W/m^2
q_{cw}	:	cold wall convective heat flux, W/m^2
q_{net}	:	net heat flux, W/m^2
$\dot{S}$	:	surface recession rate, m/s
T	:	temperature, K
T_{b_max}	:	maximum back surface temperature, K
T_{ref}	:	300K
T_{s_max}	:	maximum surface temperature, K
t	:	thickness or time, m or s
t_{ne}	:	necessary thickness of ablator, m
t_{neALL}	:	$t_{ne}+L_2$, m
t_q	:	heating duration time, s
x	:	moving coordinate or in-depth distance from receding surface, y-ΔS, m
y	:	stationary coordinate or in-depth distance from initial front surface, m
Δh_{pyro}	:	heat of pyrolysis per gas produced, J/kg
Δm	:	mass loss, kg/m^2
ΔS	:	surface recession, m
ε	:	surface emissivity
ϕ_{blow}	:	blowing correction factor
ρ	:	density, kg/m^3
σ	:	Stefan-Boltzmann constant, 5.67×10^{-8} W/(m^2 K^4)

Subscripts

ab, ch	:	ablation and char, respectively
g, ne	:	pyrolysis gas and necessary, respectively
r, ref	:	recovery and reference, respectively
u	:	at wall underside
v	:	virgin material
w	:	at wall
1, 2	:	ablator and backup wall, respectively

1. Introduction

A re-entry capsule has a heat shield system to protect inner equipment against the severe heating environment during re-entry. The heat shield system is mainly consisted of an ablator which has the capability to prevent conduction of heat to the inside by an ablation phenomenon. Until now various kinds of ablative materials with various densities have been developed. [1-8]

In the design of a heat shield system of a re-entry vehicle, a light-weight requirement on the ablator is very critical. The thickness constraint on the ablator is also important. For the design of a heat shield system, it is very important to evaluate quantitatively the heat shield performance such as necessary thickness, necessary mass, etc. with respect to the heat load, ablator density, the backup structure and so on.

Recently, a lightweight ablator named LATS (Lightweight Ablator series for Transfer vehicle Systems) with the densities of about 300-700kg/m^3 has been developed.[9] The LATS is a carbon phenolic ablator fabricated by impregnating a phenolic resin into a felt made of carbon fibers. The material properties of the LATS ablator were measured and arc-heated tests of the ablator samples with various densities were carried out. [9, 10] Ablation analysis with respect to the arc-heated tests was also carried out using a one-dimensional analysis code and the measured and calculation results agreed well.[10, 11]

Investigations concerning the effects of heat load and ablator density upon the necessary thickness t_{ne} and necessary mass m_{ne} of the LATS ablator were carried out using a one-dimensional ablation analysis code.[11] It was found that the necessary thickness t_{ne} is nearly constant as the ablator density changes, and the necessary mass m_{ne} increases almost linearly with the increase of the density. In the study, the ablator back surface was assumed to be attached to an insulation material, and the heating level was from 1 to 3 MW/m^2, which means that the surface ablation is mainly in the diffusion controlled oxidation region and not in the sublimation region (See 3.1.4.). In the study, effects of (1) a high heat flux which corresponds to the surface ablation of sublimation, (2) a constant accumulated heat load Q with a variable heat flux q, and (3) the backup wall, upon the thermal protection performance of the ablator were not investigated yet.

In this paper the effects of heat load, ablator density, backup structure, etc. upon the thermal protection performance of the LATS ablator such as the necessary thickness and the necessary mass of the ablator are investigated using a one-dimensional ablation analysis code. Heat flux time histories of a rectangular pattern are assumed. The research items of (1)-(3) mentioned above are mainly investigated in this study and are described below.
(1) Effect of a high heat flux with a constant duration time which corresponds to the surface ablation of sublimation (Sec. 3.1)

In this paper, the heat flux rate q is assumed to be from 1 to 10MW/m^2 with a constant duration time t_q of 60s. In the previous research [11], q was assumed to be from 1 to 3MW/m^2 with t_q of 60s. In such a low heating level, the surface temperature is well below 3000K and the surface ablation is mainly in the diffusion controlled oxidation region.[12, 13] If q is on the level of about 10MW/m^2, the ablator surface temperature is on the level of about 3000K, which means that the surface ablation is in the sublimation region and the surface recession would become much larger than that in the diffusion controlled oxidation region or reaction controlled oxidation region. This behavior would influence the thermal protection performance of the ablator.
(2) Constant accumulated heat load Q with a variable heat flux q (Sec. 3.2)

The effects upon the heat protection performance in the case of a constant heat load Q (120 to 600MJ/m^2) with a variable heat flux q (1 to 10MJ/m^2) are investigated. In an arc-heated test of ablative materials, heat load of a rectangular pattern is sometimes applied to the ablator, where heat flux rate q and the accumulated heat load Q ($=q*t_q$) are equal to the maximum heat flux and the accumulated heat load of the estimated re-entry heating environment, respectively. The study results would be useful for not only designing the heating conditions of an arc-heated test but also designing the heat load of re-entry vehicle and obtaining the basic knowledge of the effects of Q with variable q upon the heat protection performance of the ablator.
(3) Backup wall (Sec. 3.3 and Sec. 3.4)

Each material of the backup walls is assumed to be aluminum, stainless steel and high density CFRP, respectively. To obtain the effect of backup wall materials, two cases are studied: constant wall thickness (Sec.3.3) and constant wall mass density (Sec.3.4). The results would give valuable information in designing the candidate material of the backup wall of the heat shield system.

2. Analysis

We carried out one-dimensional ablation analysis of the LATS ablators with and without a backup wall for heating conditions of a rectangular pattern, from which the heat resistant performance of the LATS ablators with respect to the ablator densities, thicknesses, heat fluxes, accumulated heat loads and backup walls was evaluated quantitatively. Mathematical model of ablation, input data for the ablation analysis and the analysis conditions for the parametric study are shown in the following sections.

2.1. Mathematical model of ablation [10, 11]

A one-dimensional computer code for charring ablation and thermal response analysis was used to calculate the heat resistant performance of the LATS ablators. The code was developed for simulation of one-dimensional transient thermal behavior of charring materials, and was successfully applied to the LATS ablators under the heating environments of arc-heated test.[10] The mathematical model used in the code is described precisely in the previous papers. [10, 11] Thermal model of the analysis in this paper is shown in Fig. 1. In the following, the basic equations and

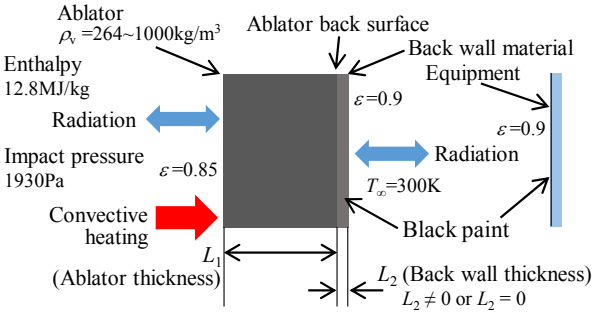

Fig. 1. Thermal model for the analysis.

boundary conditions are briefly described.

The basic equations about the charring ablation are well known.[10–16] The in-depth governing equations for one-dimensional charring ablator response are energy, mass continuity, and decomposition equations, and are expressed by

$$\rho C_{\mathrm{P}} \left.\frac{\partial T}{\partial t}\right|_x = \frac{\partial}{\partial x}\left(k\frac{\partial T}{\partial x}\right)_t + \Delta h_{\mathrm{pyro}} \left.\frac{\partial \rho}{\partial t}\right|_y + \dot{S}\rho C_{\mathrm{P}} \left.\frac{\partial T}{\partial x}\right|_t + \dot{m}_{\mathrm{g}} C_{pg} \left.\frac{\partial T}{\partial x}\right|_t \tag{1}$$

$$(\partial \dot{m}_g / \partial y)_t = (\partial \rho / \partial t)_y \tag{2}$$

$$\left(\frac{\partial \rho}{\partial t}\right)_y = -\sum_{k=1}^{N} A_k f_k (\rho_{\mathrm{v}} - \rho_{\mathrm{ch}}) \left(\frac{\rho - \rho_{\mathrm{ch}}}{\rho_{\mathrm{v}} - \rho_{\mathrm{ch}}}\right)^{\mu_k} \exp\left(-\frac{B_k}{T}\right) \tag{3}$$

Eq. (1) is the in-depth energy equation of the ablator, where $\dot{m}_{\mathrm{g}}$ is the gas flow rate (mass flux) and C_{pg} is the specific heat of the pyrolysis gas. Eq. (2) expresses the mass conservation when the ablator yields the pyrolysis gas. Eq. (3) expresses the Arrhenius type expression for the decomposition rate, where μ_{k} is the reaction order, A_{k} is the weighting factor, f_{k} is the collision frequency (1/s), B_{k} is the activation temperature (K). These values are assumed to be constant.[11, 12, 17] The virgin and char densities, ρ_{v} and ρ_{ch}, are considered constant. The density of the ablator ρ decreases from the value of ρ_{v} according to Eq. (3), and always takes a value between ρ_{v} and ρ_{ch}. k and C_{p} are calculated by

$$k = \omega(\rho_{\mathrm{v}} / \rho)k_{\mathrm{v}} + (1-\omega)(\rho_{\mathrm{ch}} / \rho)k_{\mathrm{ch}} \tag{4a}$$

$$\omega = (\rho - \rho_{\mathrm{ch}}) / (\rho_{\mathrm{v}} - \rho_{\mathrm{ch}}) \tag{4b}$$

$$C_{\mathrm{p}} = \omega(\rho_{\mathrm{v}} / \rho)C_{\mathrm{pv}} + (1-\omega)(\rho_{\mathrm{ch}} / \rho)C_{\mathrm{pch}} \tag{5}$$

where k_{v} and k_{ch} are the thermal conductivities of the virgin and char materials, and C_{pv} and C_{pch} are the specific heats of the virgin and char materials, respectively. Thermal properties of k_{v}, k_{ch}, C_{pv} and C_{pch} are functions of the temperature. k_{v} and k_{ch} for ablators with various densities ρ_{v} are also functions of ρ_{v}. (See Sec. 2.2.)

We assume three kinds of materials for the backup wall: aluminum (AL), stainless steel (SUS), and high density CFRP. For the calculation of the wall temperature, the classical heat conduction equation is used. As for the CFRP wall, the wall is treated as a non-ablating material, because the wall temperature is low (less than 250°C). (See Sec. 2.3.)

The energy balance at the ablator surface yields the surface boundary condition, in which aerodynamic heating, block effect of heating due to the mass ejection, radiation cooling, and enthalpy change when the char recedes, enthalpy change of pyrolysis gas and the heat conduction in the ablator are considered. We also assume that the pyrolysis gases are chemically inert with respect to the boundary layer gases.[13] Thus the surface boundary condition is obtained and is shown below [13]

$$q_{\mathrm{net}} = q_{\mathrm{cw}}(1 - h_{\mathrm{w}} / h_{\mathrm{r}})\phi_{\mathrm{blow}} - \varepsilon\sigma\left(T_{\mathrm{w}}^4 - T_{\mathrm{ref}}^4\right) - \dot{m}_{\mathrm{ab}}(h_{\mathrm{w}} - h_{\mathrm{u}}) \tag{6}$$

where h_{w} is the enthalpy of the gas adjacent to the surface, h_{r} is the recovery enthalpy of the flow, T_{w} is the temperature of the char surface, T_{ref} is 300 K, $\dot{m}_{\mathrm{ab}} (= \rho_{\mathrm{ch}}\dot{S})$ is the mass flux due to the thermochemical ablation of the char, and h_{u} is the enthalpy of the char at the surface. ϕ_{blow} is the blowing correction factor, which means the ratio of heat transfer coefficient with and without ablation mass injection into the boundary layer from the ablator surface. The factor ϕ_{blow} also means the correction (reduction) factor of heat flux due to the mass injection into the boundary layer.[13, 14]

As for the back surface boundary condition, radiation heat exchange between the back surface and the back environment is assumed.

The temperature and the density distributions in the ablator and backup wall are calculated by the use of the equations mentioned above. Calculation is carried out using the finite difference method considering the boundary conditions. For each time step, ρ is calculated by Eq. (3). Integration of Eq. (2) gives $\dot{m}_{\mathrm{g}}$ with the assumption that the pyrolysis gas flow is zero at the back surface of the ablator. T is calculated by Eq. (1), in which the calculation results of ρ and $\dot{m}_{\mathrm{g}}$ are used. The front surface condition of Eq. (6) and the back surface condition (attached to the back-up wall or exposed to the back environment) are also considered. In the calculation, $\dot{m}_{\mathrm{ab}}$ is obtained considering oxidation (reaction controlled or diffusion controlled oxidation) and sublimation of the surface char.[12, 13] $\dot{S}$ is obtained by the relation of $\dot{S} = \dot{m}_{\mathrm{ab}} / \rho_{\mathrm{ch}}$. C_{pg} and Δh_{pyro} are assumed to be constant values of 1674.6 J/(kg K) and 3.313×10^5 J/kg, respectively.[10, 11] For each time step, output parameters are obtained simultaneously for both the ablator and the backup wall.

2.2. Input data for the calculation

Input data for the calculation of the thermal behavior of the ablator model using the one-dimensional ablation analysis program include parameters such as heating environment conditions, ablator thickness and material properties. Input data for the ablator material properties are the same as those in the previous paper.[11] These data were determined based on the measured and the literature data.[4, 9-11, 13, 14, 17] Among them, thermal conductivity data of the LATS ablator were tuned based on the matching of the measured and calculated temperatures, [10, 11] in which the measured temperatures were obtained by the arc-heated tests of the ablators.

Simulations of the ablators in the arc-heated tests were carried out using the tuned data and simulation results of the surface and the back surface temperature time histories by the analysis program agreed well with the measured results. The simulation results of mass loss by the analysis program also agreed well with the measured results. [11]

2.3. Parametric study and conditions of the analysis

The LATS ablator with or without a backup wall is assumed as shown in Fig. 1. It is assumed that the backup wall is attached to the back surface of the ablator by an adhesive, where the allowable maximum temperature value of the adhesive $T_{\mathrm{b\_allow}}$ is 250°C (=523.15K=480F). [18] (The allowable maximum temperatures of the backup wall and the ablator are assumed more than $T_{\mathrm{b\_allow}}$.) Because the thickness of the adhesive is assumed to be very small, the adhesive was neglected in the analysis and the calculated ablator back surface temperature is regarded as the adhesive temperature.

T_{s_max} is the maximum back surface temperature evaluated at the end of the heating time t_q. T_{b_max} is the maximum back surface temperature which corresponds to the maximum adhesive temperature between the ablator and the backup wall. Δm is the mass loss, and ΔS is the surface recession evaluated at t=600s in Sec. 3.1 and t_q+600s in Sec. 3.2, respectively. For the time more than the evaluation time, the calculated results are approximately the same, which means that the results do not change much during the time more than the evaluation time. The necessary thickness t_{ne} or mass m_{ne} is defined to be the ablator thickness or mass per unit area in which T_{b_max} is equal to T_{b_allow}. t_{neALL} or m_{neALL} is also defined to be the necessary thickness or mass added by the wall thickness L_2 or the wall mass m_2, and expressed by t_{neALL}= t_{ne}+L_2 or m_{neALL} = m_{ne}+m_2, respectively.

T_{s_max}, T_{b_max}, Δm, and ΔS are calculated as functions of virgin density ρ_v, ablator thickness L_1, heat flux q, and so on. t_{ne} and m_{ne} are also calculated as functions of ρ_v, q, accumulated heat load Q and the backup wall.

Calculated parameters mentioned above are useful for various design aspects: T_{s_max} can be used for estimating the in-depth temperature, T_{b_max} can be used for the design requirement of the heat shield system, Δm is related to the mass and movement of the center of gravity of the re-entry vehicle, ΔS influences the aerodynamic characteristics of the re-entry vehicle, and t_{ne} and m_{ne} influence the outer geometry and the mass of the re-entry vehicle, respectively. Among these parameters, t_{ne} and m_{ne} seem to be most important with respect to the heat shield design.

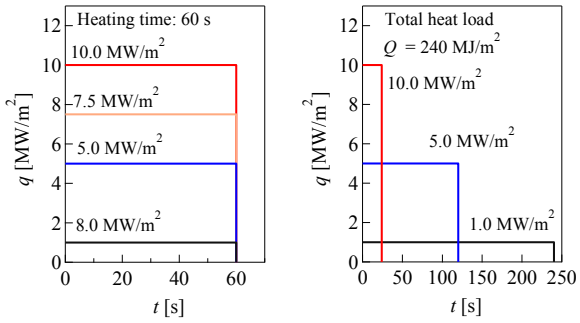

(a) t_q =const. (b) Q=const.

Fig. 2. Examples of heat flux time histories.

Table 1. Conditions of Analysis

Section 3.1 Constant heating duration time	
Heat Load	q=1~10MW/m^2, t_q=60s
Backup wall	L_2=0, 2× 10^{-3}m (material: AL)
Section 3.2 Constant accumulated heat load	
Heat Load	Q=120~600MJ/m^2, q=1~10 MW/m^2
Backup wall	L_2=0, 2× 10^{-3}m (material: AL)
Section 3.3 Effect of backup wall material (constant wall thickness L_2 and constant heating duration time t_q)	
Heat Load	q=1~10 MW/m^2, t_q=60s
Backup wall material	AL, SUS, CFRP (L_2=2× 10^{-3}m)
Section 3.4 Effect of backup wall material (constant wall mass density m_2 and constant heating duration time t_q)	
Heat Load	q=1~10 MW/m^2, t_q=60s
Backup wall material	AL, SUS, CFRP (m_2=5.4kg/m^2)

For the parametric calculation, heat flux time histories of rectangular patterns of constant heating duration time and constant accumulated heat load are considered, examples of which are shown in Fig. 2. The rectangular heating pattern is usually used in the arc-heated test of ablators. The heating level is assumed to be from 1 to 10MW/m^2, which corresponds to the regions of diffusion controlled oxidation/ sublimation (see 3.1.4.). The impact pressure of 1930 Pa and enthalpy of 12.8 MJ/m^2, the values of which are derived from those of the arc-heated test shown in Sec. 2.2, are used for the calculation. The ablator virgin density ρ_v is assumed to be from 264 to 1000 kg/m^3. The char density is calculated by [9, 11]

$$\rho_{ch} = \rho_v \times 0.7 \tag{7}$$

Material properties of AL and SUS used for the analysis are based on the literature. [19, 20] Material properties of the high density CFRP are estimated by means of those of the LATS ablator.

The emissivity of the front surface is taken as ε=0.85. [10, 11] The back surface and equipment in the back environment are assumed to be painted black, where radiant heat exchange between the back surface and the equipment in the back environment is assumed. The radiant energy flux is calculated by assuming the radiation between parallel plates, in which the emissivity of the back surface and back environment was assumed to be 0.9 and 0.9, respectively. (The emissivity of the black painted surface is assumed to be 0.9)

Conditions of the analysis are shown in Fig. 1 and Table 1. In this paper, Sec. 3.1 is regarded as a baseline section, where various calculated parameters are evaluated. In other sections of 3.2 - 3.4, important parameters of necessary thickness and mass are evaluated, and other parameters are omitted. (Sec. 3.2 includes also T_{b_max}, which is related to the necessary thickness and mass.)

3. Results and Discussion

Effects of heat load, ablator density, backup structure, etc. upon the thermal protection performance of the LATS ablators such as the necessary thickness and necessary mass of the ablator system are investigated using a one-dimensional ablation analysis code.

3.1. Constant heating duration time

In this section, thermal protection performance of the LATS ablator is examined for a constant t_q of 60s with or without an aluminum backup wall of L_2=2× 10^{-3}m, with the heat flux q of 1 to 10MW/m^2.

3.1.1. Maximum surface temperature T_{s_max}

Figure 3a shows the relation between the maximum surface temperature T_{s_max} and ρ_v for various values of heat flux q with a constant t_q of 60s. It is seen that for q=5, 7.5 and 10MW/m^2, T_{s_max} is nearly constant independent of the values of ρ_v, whereas T_{s_max} decreases slightly as ρ_v increases for q=1MW/m^2. Figure 3b shows the relation between T_{s_max} and q for several values of ρ_v. T_{s_max} increases as q increases. Deviations of T_{s_max} due to the density decrease as q increases.

Additional calculations show that longer t_q of more than 60s

tends to raise T_{s_max} especially for high ρ_v and low q in Fig. 3a, and each curve of constant q approaches the parallel line with respect to the ρ_v axis. This means that the ablator is not in a steady state condition but is still in a transient condition especially for high ρ_v and low q. Deviations of T_{s_max} due to the density which is shown in Fig. 3b also decrease as t_q increases.

With the following assumptions and by using a simple model, we can show that each term of surface energy balance equation Eq. (6) is the same irrespective of the ablator density, which is shown below.

We assume the LATS ablators with various densities, and that each ablator is in a steady state condition under the same heating load. We also assume that the surface temperature T_s, mass loss rate of the ablator surface $\dot{m}_{ab}$, mass loss rate of the pyrolysis gas $\dot{m}_g$ and total mass loss rate $\dot{m}_w(=\dot{m}_{ab}+\dot{m}_g)$ of each ablator are the same, respectively. (It can be shown by simple consideration that these assumptions of a steady state condition, and the same heating load, T_s and mass loss rate do not contradict each other.)

When we assume the assumptions mentioned above, each term on the right side of Eq. (6) has the same value for different densities, because each term is a function of the heat load/surface temperature/mass loss rate, and not of the ablator density.[13] The term of left side means the net heat conduction into the ablator, which is roughly approximated by using a simple model of a steady state semi-infinite receding solid of constant properties with constant T_s, T_i (initial temperature), and mass loss rate. Thus we obtain $q_{net}=\dot{m}_{ab}C_p(T_s-T_i)$.[21] Assuming C_p is the same, this relation means the same value of q_{net} for different densities.

The above results, although roughly estimated, do not contradict the tendency that the surface temperature is nearly equal irrespective of the ablator density, as shown in Figs. 3a and 3b.

3.1.2. Maximum back surface temperature T_{b_max}

Figures 4a and 4b show the relations between T_{b_max} and ρ_v with and without an aluminum backup wall of L_2=2× 10^{-3}m, for q=1 and 10MW/m^2, with L_1 of 40×10^{-3} and 60×10^{-3}m, respectively.

In both figures, for low q, T_{b_max} is nearly constant with various ρ_v. Main factors that influence T_{b_max} would be the thermal diffusivity of the ablator α and the surface recession ΔS.[11] α of the LATS ablator is nearly equal for different densities (For example, the difference of α between ρ_v=400 and 1000kg/m^3 is about 10%.). When ΔS is relatively small, nearly equal α determines nearly equal T_{b_max}. Low q yields relatively small ΔS (See 3.1.4.) and nearly equal T_{b_max} is obtained.

It is seen that T_{b_max} slightly increases as ρ_v increases for low q, the reason of which would be due to the combination of small ΔS, nearly equal α, and other factors of the surface temperature T_s (during heating) and the heat capacity ρC_p. (For precise discussion of the mechanism, see Ref. 11).) It is seen that the dependency of T_{b_max} upon ρ_v is smaller when q is lower, L_1 is larger and ρ_v is larger. Lower q, larger L_1 and larger ρ_v correspond to relatively smaller ΔS (See 3.1.4.), which contribute the small dependency of T_{b_max} upon ρ_v. It is also seen that T_{b_max} increases when q increases, L_1 decreases, or the backup wall is not attached. Larger q and smaller L_1 correspond

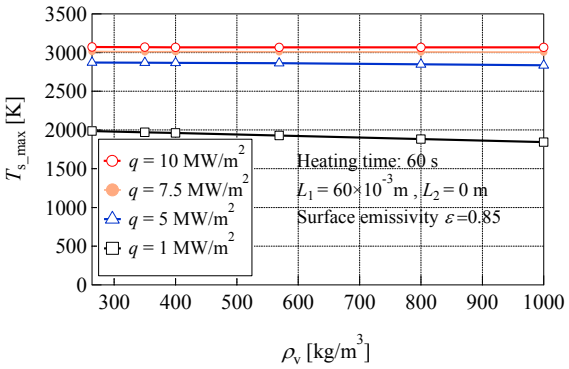

Fig. 3a. Relation between T_{s_max} and ρ_v for various q.

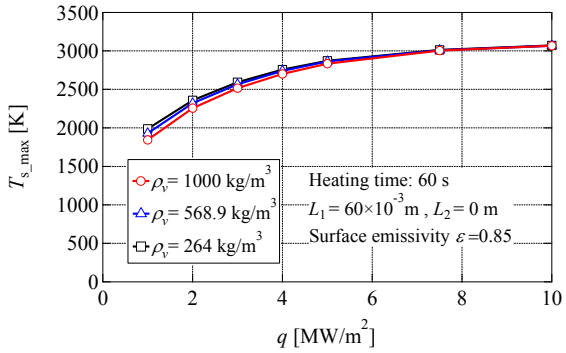

Fig. 3b. Relation between T_{s_max} and q for various ρ_v.

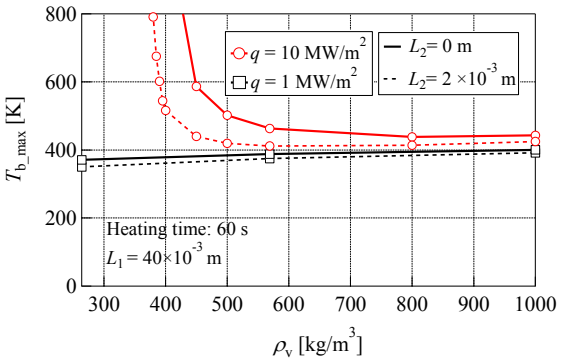

Fig. 4a. Relation between T_{b_max} and ρ_v.

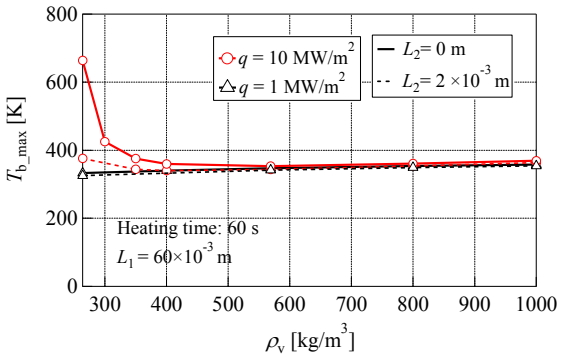

Fig. 4b. Relation between T_{b_max} and ρ_v.

to relatively larger ΔS, which contribute to increase T_{b_max}. As for the backup wall, the wall heat capacity decreases T_{b_max}. In these figures, with q=10MW/m^2, T_{b_max} increases rapidly as ρ_v decreases in the range of low density. In this case, ΔS increases largely for a low density ablator, which increases T_{b_max}.

3.1.3. Mass loss of ablator Δm

Figure 5 shows the relation between the mass loss Δm and ablator density ρ_v with several q for t_q of 60s. It is seen that Δm increases almost linearly as ρ_v increases. In the previous paper [11] it was shown that for a relatively low value of q with diffusion controlled oxidation, the mass loss Δm ($=\Delta m_{ab\_d}+\Delta m_g$, Δm_{ab_d}: mass loss of surface recession due to diffusion controlled oxidation, Δm_g: mass loss due to pyrolysis gas) has a linear relation with ρ_v by using a simple model. For a high value of q, additional effect of sublimation should be considered. In the sublimation range, when q is the same, each surface temperature of ablators with different densities is nearly equal (See 3.1.1.). The same surface temperature gives the same mass loss due to sublimation.[13] Thus the mass loss of surface recession due to sublimation Δm_{ab_s} is also the same, which means that the relation of Δm ($=\Delta m_{ab\_d}+\Delta m_g+\Delta m_{ab\_s}$) and ρ_v is also linear in the sublimation region.

3.1.4. Surface recession ΔS

Figure 6a shows the relations between the surface recession of the ablator ΔS and ρ_v with several q for t_q of 60s. Figure 6b shows the relation between ΔS and q with several ρ_v. In these figures, solid curves ($\Delta S_{d/s}$) are calculated considering diffusion controlled oxidation/sublimation [12, 13] and dotted curves (ΔS_d) are calculated considering only diffusion controlled oxidation. It is seen that $\Delta S_{d/s}$ increases with the decrease of ρ_v or the increase of q. When q is higher and ρ_v is lower, $\Delta S_{d/s}$ increases largely. For low q the difference between $\Delta S_{d/s}$ and ΔS_d is small, which means that the surface recession is mainly due to diffusion controlled oxidation. For high q, the difference between $\Delta S_{d/s}$ and ΔS_d becomes larger, which means that the effect of sublimation upon the surface recession becomes larger and the surface recession is promoted.[12, 13]

3.1.5. Necessary thickness t_{neALL}

Figure 7 shows the relation between the necessary thickness of the ablator t_{neALL} and the density ρ_v for various q of a constant heating time t_q of 60s, with and without an aluminum backup wall of $L_2=2\times 10^{-3}$m. (Necessary thickness t_{neALL} is defined to be $t_{neALL} = t_{ne} + L_2$.) t_{neALL} increases with the increase of q.

The dependency of t_{neALL} upon ρ_v is small for q=1 and 5MW/m^2. Considering the tendency of t_{neALL} is the same as that of T_{b_max} in 3.1.2, the reason of small dependency on ρ_v is due to small ΔS and nearly equal α as shown in 3.1.2.

For q=1 and 5MW/m^2 with more than about 600kg/m^3, t_{neALL} is seen to increase slightly as ρ_v increases. The slight increase would be due to the combination of a relatively small value of ΔS, nearly equal α and other factors of surface temperature and heat capacity of the ablator as described in 3.1.2.

For q=10MW/m^2, t_{neALL} increases monotonously as the density decreases. The increasing rate also increases as the density decreases. The reason why t_{neALL} is large especially for low density and high heat flux is as follows: When ρ_v is lower and q is higher, ΔS increases. Especially when q is around 10MW/m^2, the surface recession increases largely due to the combination of diffusion controlled oxidation and sublimation, which causes the thickness of the ablator shorter, and t_{neALL} becomes larger. This tendency is slightly seen also with q=5MW/m^2 for low density.

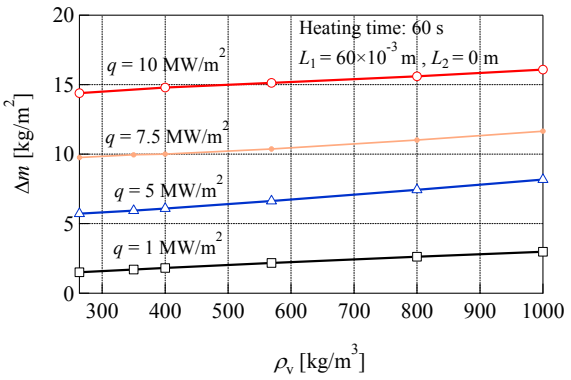

Fig. 5. Relation between Δm and ρ_v for several value of q.

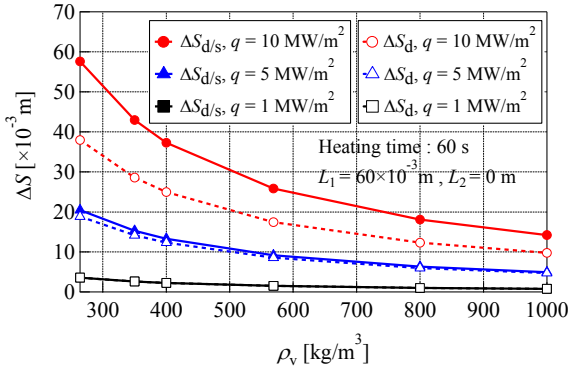

Fig. 6a. Relation between ΔS and ρ_v for several q.

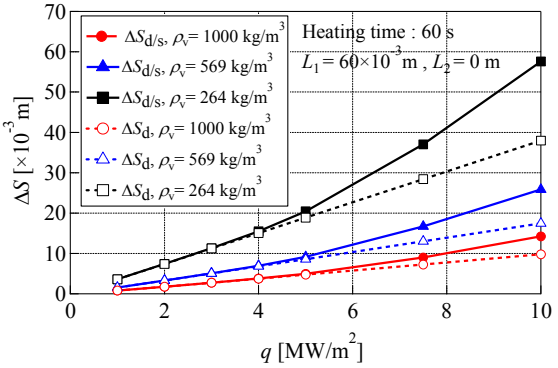

Fig. 6b. Relation between ΔS and q for several ρ_v.

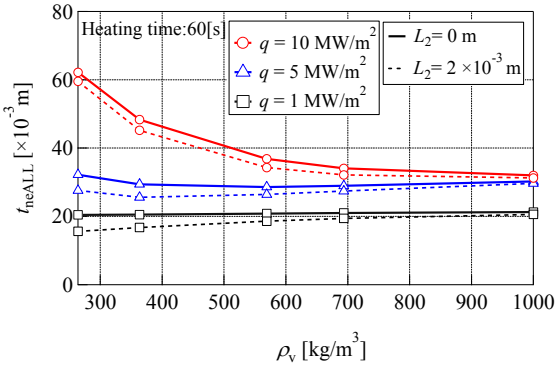

Fig. 7. Relation between t_{neALL} and ρ_v for several q.

When a backup wall is attached to the ablator, t_{neALL} decreases. (It is seen that t_{ne} decreases with a backup wall

attached.) Because L_2 has a constant value for each of the wall conditions, the tendency of t_{ne} is similar to that of t_{neALL}.

3.1.6. Necessary mass m_{neALL}

The necessary mass m_{neALL} is defined to be $m_{neALL} = m_{ne} + m_2$, where m_{ne} is the necessary mass expressed by $m_{ne} = t_{ne}\rho_v$ and m_2 is the wall mass expressed by $m_2 = L_2\rho_2$. Accordingly, m_{neALL} is expressed by

$$m_{neALL} = t_{ne}\rho_v + L_2\rho_2 \quad (8)$$

When L_2 is constant, $L_2\rho_2$ (= m_2) also has a constant value for the same wall material. Eq. (8) means that t_{ne} determine the value of m_{neALL}. So, t_{neALL}(=t_{ne}+L_2) in Fig. 7 determines m_{neALL}. Figure 8 shows the relations between the necessary mass of the ablator m_{neALL} and the virgin density ρ_v with several kinds of q for a constant heating time t_q of 60s, with and without an aluminum backup wall of L_2=2× 10^{-3}m. It is seen that m_{neALL} increases as ρ_v increases, and the relation is nearly linear for the low heat flux. For low q, t_{neALL} (t_{ne}) is nearly constant in Fig. 7, which gives the nearly linear relation of m_{neALL} and ρ_v in Fig. 8. While as shown in Fig. 7, t_{neALL} (and t_{ne}) with q=10MW/m^2 decreases as ρ_v increases in the low density region, m_{neALL} (and m_{ne}) increases as ρ_v increases. This is because m_{ne} is the product of t_{ne} and ρ_v. It is also seen that m_{neALL} increases as q increases. When ρ_v is high, the value of m_{neALL} for q=5 MW/m^2 is relatively near that for 10MW/m^2. This tendency corresponds to that of t_{neALL} shown in Fig. 7. When an aluminum backup wall is attached to the ablator, m_{neALL} increases (Based on Fig. 7, it is also seen that m_{ne} decreases with a backup wall attached).

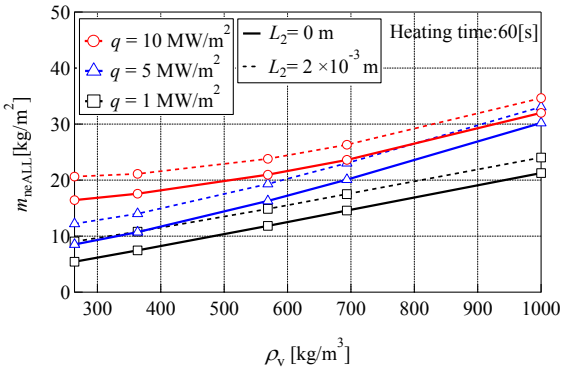

Fig. 8. Relation between m_{neALL} and ρ_v for several q.

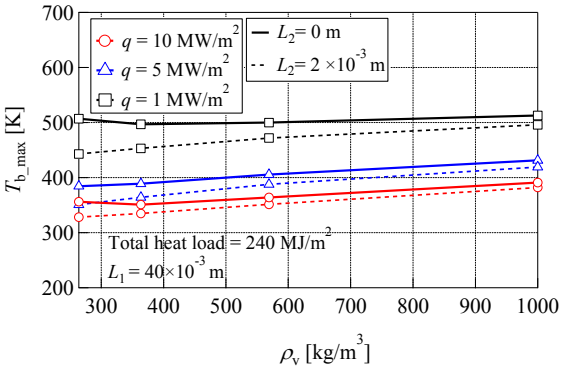

Fig. 9. Relation between T_{b_max} and ρ_v for a constant heat load (Q=240MJ/m^2, L_1=40×10^{-3}m).

Because m_2 has a constant value for each of the wall conditions, the tendency of m_{ne} is similar to that of m_{neALL}.

In order to satisfy the back surface temperature requirement, selection of a lower density ablator is more advantageous than that of a higher density ablator from the point of reducing the ablator mass. However, selection of a low density ablator gives a larger necessary thickness.

3.2. Constant accumulated heat load

In this section, thermal protection performance of the LATS ablator is examined for the case of constant accumulated heat load Q (Q=q*t_q) from 120 to 600MJ/m^2, where q is from 1 to 10MW/m^2 and t_q is calculated by t_q=Q/q.

3.2.1. Maximum back surface temperature T_{b_max}

Figure 9 shows the relation between T_{b_max} and ρ_v of the ablator of L_1=40 × 10 $^{-3}$m, with and without an aluminum backup wall of L_2=2× 10^{-3}m, for Q of 240 MJ/m^2 with several q. It is seen that T_{b_max} decreases as q increases. For constant Q, when q is lower or higher, t_q becomes longer or shorter, respectively. Different q and t_q give different temperature distributions in the ablator. This would be the reason of the relation between T_{b_max} and q. When a backup wall is attached, T_{b_max} decreases. Dependency of T_{b_max} upon ρ_v is not so large for a constant value of q, the main reason of which would be relatively small value of ΔS, and nearly equal α for different densities (See 3.1.2.)

3.2.2. Necessary thickness t_{neALL}

Figures 10a and 10b show the relations between the necessary thickness of the ablator t_{neALL} and ρ_v with and without

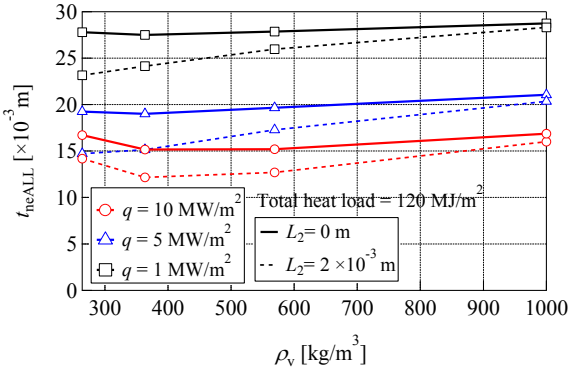

Fig. 10a. Relation between t_{neALL} and ρ_v (Q=120MJ/m^2).

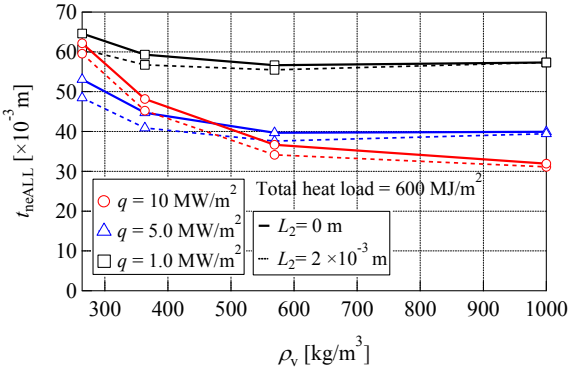

Fig. 10b. Relation between t_{neALL} and ρ_v (Q=600MJ/m^2).

an aluminum backup wall of L_2=2× 10^{-3}m with several q, for Q of 120 and 600 MJ/m^2 respectively. In Fig. 10a, it is seen that for a constant Q of 120MJ/m^2, at least except for the case of low density, t_{neALL} decreases as q increases. t_{neALL} also decreases when a backup wall is attached. In Fig. 10b, it is seen that for a constant Q of 600MJ/m^2, t_{neALL} decreases as q increases for relatively high density ablators. In the range of relatively low density, t_{neALL} decreases as ρ_v increases. Except for the case of ρ_v=1000kg/m^3, t_{neALL} decreases when a backup wall is attached. (t_{ne} also decreases with a backup wall attached.) In both figures, t_{neALL} decreases as q increases with the exception of some conditions. As mentioned in 3.2.1, this would be because of the different temperature distributions in
the ablator due to the different q and t_q. In Fig. 10b, t_{neALL} in the

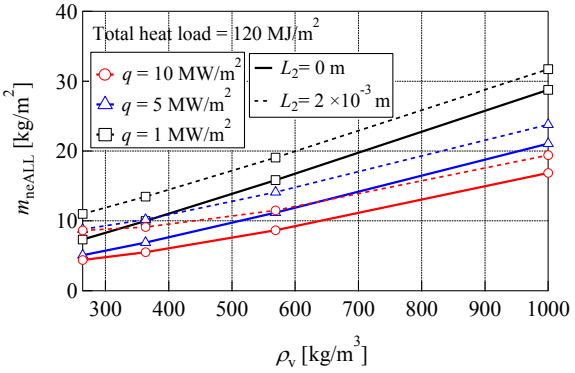

Fig. 11a. Relation between m_{neALL} and ρ_v (Q=120MJ/m^2).

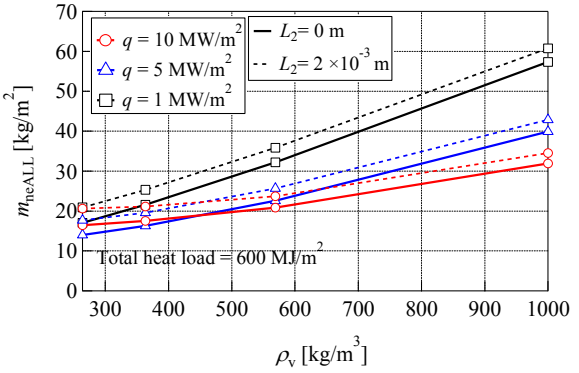

Fig. 11b. Relation between m_{neALL} and ρ_v (Q=600MJ/m^2).

low density region increases for high q, the reason of which would be due to the large surface recession in this region.

Because L_2 has a constant value for each of the wall conditions, the tendency of t_{ne} is similar to that of t_{neALL}.

3.2.3. Necessary mass m_{neAL}

Figures 11a and 11b show the relations between the necessary mass m_{neALL} and ρ_v with and without an aluminum backup wall of L_2=2× 10^{-3}m with several q for Q of 120 and 600 MJ/m^2, respectively. In Fig. 11a, it is seen that for Q= 120MJ/m^2, m_{neALL} increases as ρ_v increases. When a backup wall is attached, m_{neALL} increases. (Based on Figs. 10a and 10b, it is also expected that m_{ne} decreases when a backup wall is attached.) Except for the case of very low density, m_{neALL} decreases as q increases. In Fig. 11b, it is seen that with Q=600MJ/m^2, for a relatively high density ablator m_{neALL} increases as ρ_v increases, q decreases or when a backup wall is

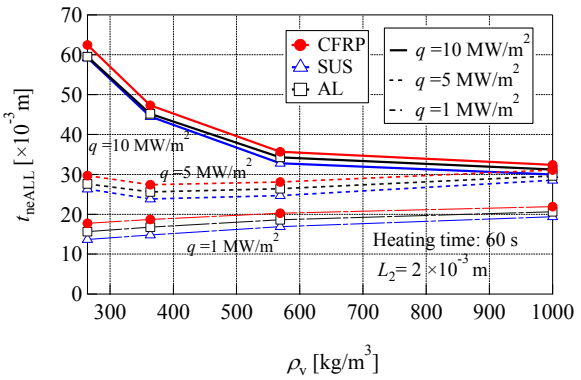

Fig. 12. Relation between t_{neALL} and ρ_v (t_q=60s, L_2=2×10^{-3}m).

attached.

In both figures, except for some conditions m_{neALL} decreases as q increases. As discussed in 3.2.1 and 3.2.2, this would be because of the different temperature distributions in the ablator due to the different q and t_q. It is also seen that, m_{neALL} increases as ρ_v increases, the tendency of which is different from that of Fig. 10a or 10b. As discussed in Sec. 3.1.6, this is because m_{ne} is the product of t_{ne} and ρ_v.

Because m_2 has a constant value for each of the wall conditions, the tendency of m_{ne} is similar to that of m_{neALL}.

3.3. Effect of backup wall material (constant wall thickness L_2 and constant heating duration time t_q)

Figure 12 shows the relation between the necessary thickness t_{neALL} and ρ_v for various q with t_q of 60s, with backup walls of L_2=2×10^{-3}m, materials of which are aluminum (AL), stainless steel (SUS), and high density CFRP. Each density of AL, SUS and CFRP is assumed to be 2713, 7833, and 1450 kg/m^3, respectively. It is seen that SUS gives the minimum thickness of t_{neALL}, AL and CFRP give the second and the third minimum, respectively for most of the parameter range. The ratios of heat capacity ρC_p of SUS and AL with respect to CFRP are, $(\rho C_p)_{SUS}/(\rho C_p)_{CFRP} \cong 2.0$ and $(\rho C_p)_{AL}/(\rho C_p)_{CFRP} \cong 1.4$ (average values between RT and 250°C) respectively, from which SUS has the maximum heat capacity. The maximum heat capacity of a wall gives the minimum t_{ne} and thus t_{neALL}. This is the reason why SUS gives the minimum t_{neALL}.

t_{neALL} is expressed by t_{neALL}= t_{ne} + L_2 and L_2 is constant (2× 10^{-3}m). This means that the tendency of t_{ne} is similar to that of t_{neALL}.

Figure 13a shows the relation between m_{ne} and ρ_v for various q with t_q of 60s, with backup walls of L_2=2× 10^{-3}m, materials of which are AL, SUS, and CFRP. It is seen that SUS gives the minimum m_{ne}. AL and CFRP give the second and the third minimum, respectively for most of the parameter range.

Figure 13b shows the relation between m_{neALL} and ρ_v for various q with t_q of 60s, with backup walls of L_2=2× 10^{-3}m, materials of which are AL, SUS, and CFRP. It is seen that CFRP gives the minimum m_{neALL}, and AL and SUS give the second and the third minimum, respectively for most of the parameter range. Although m_{ne} for CFRP is the maximum and that for SUS is the minimum as shown in Fig. 13a, the wall mass m_2 (=$\rho_2 L_2$) of CFRP is the minimum and that of SUS is the maximum. Thus, m_{neALL} (=m_{ne}+m_2) of CFRP becomes the minimum and that of SUS becomes the maximum.

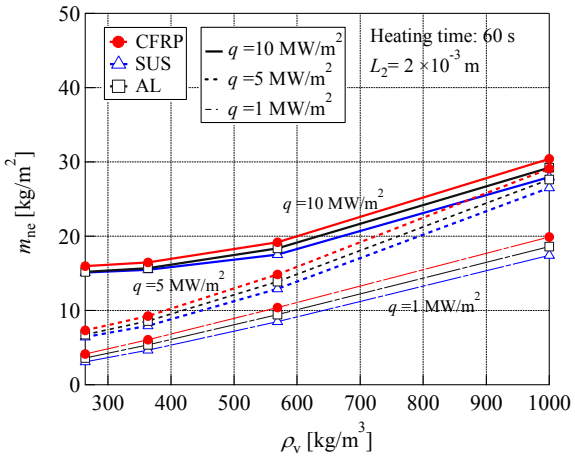

Fig. 13a. Relation between m_{ne} and ρ_v for three kinds of wall materials (t_q=60s, L_2=2×10^{-3}m).

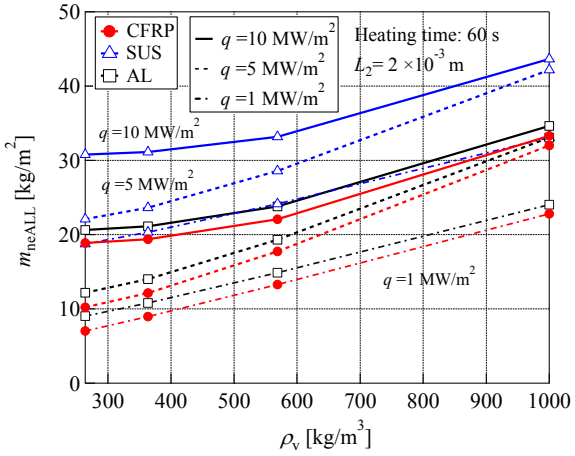

Fig. 13b. Relation between m_{neALL} and ρ_v for three kinds of wall materials (t_q=60s, L_2=2×10^{-3}m).

3.4. Effect of backup wall material (Constant wall mass density m_2 and constant heating duration time t_q)

Figure 14 shows the relation between t_{ne} and ρ_v for various q with t_q of 60s, with backup walls of m_2=5.4kg/m^2. The thickness L_2 of each material of AL, SUS, and CFRP is 2× 10^{-3}, 0.693× 10^{-3} and 3.74× 10^{-3}m, respectively. It is seen that CFRP gives the minimum t_{ne}, AL and SUS give the second and the third minimum, respectively for most of the parameter range. Because the wall mass density m_2 is the same for each material, specific heat of the material plays an important role for the necessary thickness. The ratio of specific heat C_p of SUS and AL with respect to CFRP is, $(C_p)_{SUS}/(C_p)_{CFRP} \cong 0.4$, $(C_p)_{AL}/(C_p)_{CFRP} \cong 0.7$ (average values between RT and 250°C), from which CFRP has the maximum specific heat. The maximum specific heat gives the minimum t_{ne}. This is the reason why CFRP gives the minimum t_{ne}.

Figure 15 shows the relation between the necessary mass of the ablator m_{ne} and ρ_v for various q with t_q of 60s, with a backup wall of m_2=5.4kg/m^2, each material of which is AL, SUS, and CFRP, respectively. It is seen that CFRP gives the minimum m_{ne}, AL gives the second minimum and SUS gives the third minimum, for most of the parameter range.

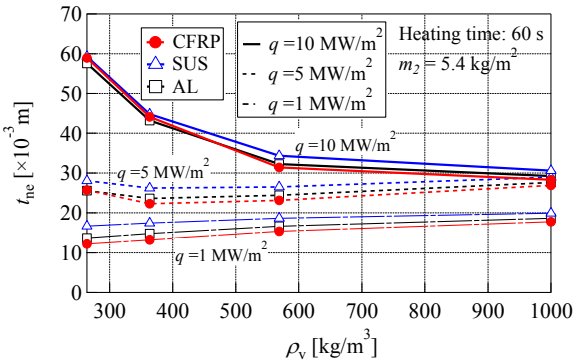

Fig. 14. Relation between t_{ne} and ρ_v for three kinds of wall materials (t_q=60s, m_2=5.4kg/m^2).

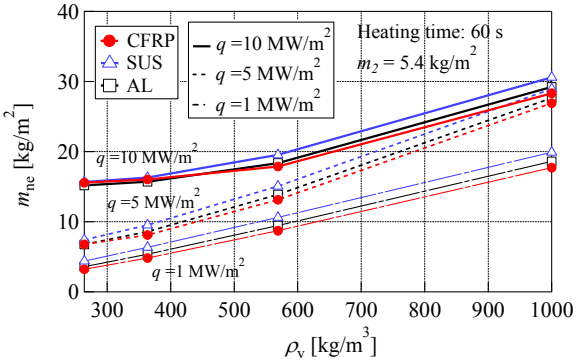

Fig. 15. Relation between m_{ne} and ρ_v for three kinds of wall materials (t_q=60s, m_2=5.4kg/m^2).

Because m_2 is the same for each material, the tendency of m_{neALL} is similar to that of m_{ne} in Fig.15.

3.5. Important results of the analysis

Among the calculated parameters, the thickness and mass of the ablator system is very important in the design of the heat shield system. Here, main results of the analysis with respect to the necessary thickness and mass are summarized as follows:

(1) When a backup wall is attached, t_{ne} and t_{neALL} decrease and m_{neALL} increase for most of the parameter range.

(2) For a low heating level with a constant t_q, t_{ne} is nearly constant as the density changes. On the other hand, t_{ne} increases largely when q is larger and ρ_v is smaller. m_{ne} increases with the increase of ρ_v and q.

(3) For a constant Q, t_{ne}, t_{neALL}, m_{ne} and m_{neALL} decrease for a higher q especially when ρ_v is high.

(4) When L_2 is the same, the CFRP backup wall gives the minimum m_{neALL}, but gives the maximum t_{neALL} (and t_{ne}) for most of the parameter range. The SUS wall gives the maximum m_{neALL}, and the minimum t_{neALL} (and t_{ne}).

(5) When m_2 is the same, the CFRP backup wall gives the minimum m_{ne} (and m_{neALL}) and minimum t_{ne} for most of the parameter range. The SUS wall gives the maximum m_{ne} (and m_{neALL}) and the maximum t_{ne}.

(6) Selection of a lower density ablator with a CFRP backup wall is more advantageous than that of a higher density ablator with other walls (AL, SUS) from the point of mass reduction of the heat shield system for most of the parameter range.

(7) For a high heat flux, selection of a lower density ablator gives a larger necessary thickness.

In the previous study [11] with a relatively low heating load (region of diffusion controlled oxidation), it was found that the calculated results of thermal protection performance of the LATS ablator based on the arc-heated test conditions (rectangular heating pattern) are similar to those based on the re-entry conditions. The study in this paper is based on the high heating load of a rectangular pattern (arc-heated test heating condition), which includes the region of sublimation. The surface degradation mechanisms of diffusion controlled oxidation and sublimation are quite different. Therefore it is not so clear that the study results of this paper based on the high heating load of a rectangular pattern would be similar to those based on the re-entry conditions, as in the case of low heating conditions. [11] This should be confirmed in the future study.

4. Conclusions

Main findings within the range of parameters investigated in this paper are:
(1) The dependency of the maximum surface temperature upon the ablator density is small especially when q is high.
(2) The dependency of the maximum back surface temperature T_{b_max} upon the ablator density is small especially for a large ablator thickness, a low heat flux and a high density, whereas for a small thickness, a large heat flux and a low density, T_{b_max} increases largely especially when the ablator density is small.
(3) For high q, the effect of sublimation upon the surface recession is relatively large.
(4) The main results of the analysis with respect to the necessary thickness and mass are summarized in Sec. 3.5.

The study results in this paper would give important information in selecting, designing and testing the candidate ablator to be used for the heat shield system of a newly developed re-entry capsule in the near future.

Acknowledgement

The authors are deeply grateful to the people of, JAXA and Nagoya Univ. for their support to our research.

References

1) Strauss, E. L.: Superlight Ablative Systems for Mars Lander Thermal Protection, Journal of Spacecraft and Rockets, **4** (1967), No. 10, pp.1304-1309.
2) Sutton, K.: An experimental study of a carbon-phenolic ablation material, NASA TN D-5930, Sept. 1970.
3) Peterson, D. L. and Nicoleit, W. E.: Heat Shielding for Venus Entry Probes, Journal of Spacecraft and Rockets, **11** (1974), No. 6, pp. 382-387.
4) Tran, H., Johnson, C., Rasky, D., Hui, F., Chan, Y. K. and Hsu, M.: Phenolic Impregnated Carbon Ablators (PICA) for Discovery Class Missions, AIAA-96-1911, 31st AIAA Thermophysics Conference, June 1996.
5) Milos, F. S., Chen, Y.-K. and Squire T. H.: Analysis of Galileo Probe Heat Shield Ablation and Temperature Data: Ablation and Thermal Response Program for Spacecraft Heatshield Analysis, Journal of Spacecraft and Rockets, **36** (1999), No. 3, pp. 298-306.
6) Kato, S., Sakata, R., Kanno, Y., Uto, M., Okuyama, K., Uegaki, E., Shingu, S., Ijichi, K. and Inatani, Y.: Development of USERS/REM Heat Shield System and its Evaluation after Re-entry, ISTS2004-e-36, Proceedings of the 24th International Symposium on Space Technology and Science (Selected Papers), Miyazaki, Japan, 2004, pp. 621-628.
7) Kontinos, D. A. and Stackpoole, M.: Post Flight Analysis of the Stardust Sample Return Capsule Earth Entry, AIAA-2008-1197, 46th AIAA Aerospace Sciences Meeting and Exibit, Reno, Nevada, January, 2008.
8) Yamada, T., Ishii, N. and Inatani, Y.: Post Flight Analysis of the Hayabusa Sample Return Capsule, 2011-def-03, 28th International Symposium on Space Technology and Science (28th ISTS), 5-12 June, Okinawa Prefecture, Japan.
9) Okuyama, K., Kato, S. and Ohya, H.: Thermochemical Performance of a Lightweight Charring Carbon Fiber Reinforced Plastic, Transactions of the Japan Society for Aeronautical and Space Sciences. **56** (2013), No.3, pp.159-169.
10) Kato, S., Okuyama, K., Gibo, K., Miyagi, T., Suzuki, T., Fijita, K., Sakai, T., Nishio, S. and Watanabe, A.: Thermal Response Simulation of Ultra Light Weight Phenolic Carbon Ablator by the Use of the Ablation Analysis Code, Transactions of JSASS Aerospace Technology Japan, **10** (2012), No.ists28, pp. Pe_31-Pe_39.
11) Kato, S., Kishimoto, T., Matsuda, S., Okuyama, K., Watanabe, A., and Shimada, N.: Study of the Effects of Density, Thickness and Heat Load on Heat Shielding Performance of Phenolic Carbon Ablators Using a One-Dimensional Ablation Analysis Code, Transactions of JSASS Aerospace Technology Japan, **12** (2014), No. ists29, pp.Po_2_29 - Po_2_38.
12) Kato, S., Okuyama, K., Nisio, S., Sakata, R., Hama, K., and Inatani, Y.: Numerical Analysis of Charring Ablation for Ablative Materials of Re-Entry Capsules, Journal of the Japan Society for Aeronautical and Space Sciences, **50** (2002), No.582, pp. 255-263.(in Japanese)
13) Potts, R. L: Application of Integral Methods to Ablation Charring Erosion, A Review, Journal of Spacecraft and Rockets, **32** (1995), No.2, pp. 200-209.
14) Potts, R. L.: Hybrid Integral/Quasi-Steady Solution of Charring Ablation, AIAA-90-1677, AIAA/ASME 5th Joint Thermophysics and Heat Transfer Conference, June 1990.
15) Moyer, C. B., and Rinadal, R. A.: An Analysis of Coupled Chemically Reacting Boundary Layer and Charring Ablator, Part Ⅱ, Finite Difference Solution for the In-Depth Response of Charring Materials Considering Surface Chemical and Energy Balances, NASA CR-1061, 1967.
16) Chen, Y.-K., and Milos, F. S.: Ablation and Thermal Response Program for Spacecraft Heatshield Analysis, Journal of Spacecraft and Rockets, **36** (1999), No. 3, pp. 475-483.
17) Suzuki, T., Fujita, K., Sakai, T., Okuyama K., Kato, S. and Nishio, S.: Thermal Response Analysis of Low Density CFRP Ablator, 2011-e-41, 28th International Symposium on Space Technology and Science (28th ISTS), 5-12 June 2011, Okinawa Prefecture, Japan.
18) Willcockson, W. H.: Mars Pathfinder Heatshield design and Flight Experience, Journal of Spacecraft and Rockets, **36** (1999). No. 3, pp. 374-379.
19) MIL-HDBK-5F, Nov. 1990
20) JSME Data Book: Heat Transfer, 5th Edition, 2009 (in Japanese).
21) Holman, J. P., Heat Transfer, Seventh Edition, McGraw-Hill, 1992, pp.638-640.